

Quantum-geometry-facilitated pair density wave order: Density matrix renormalization group study

Hao-Xin Wang^{1,*} and Wen Huang^{2,3,4,†}

¹*Department of Physics, The Chinese University of Hong Kong, Sha Tin, New Territories, Hong Kong, China*

²*Shenzhen Institute for Quantum Science and Engineering, Southern University of Science and Technology, Shenzhen 518055, Guangdong, China*

³*International Quantum Academy, Shenzhen 518048, China*

⁴*Guangdong Provincial Key Laboratory of Quantum Science and Engineering, Southern University of Science and Technology, Shenzhen 518055, China*

(Dated: June 26, 2024)

Understanding the formation of novel pair density waves (PDWs) in strongly correlated electronic systems remains challenging. Recent mean-field studies suggest that PDW phases may arise in strong-coupling multiband superconductors by virtue of the quantum geometric properties of paired electrons. However, confirmation via sophisticated many-body calculations has been lacking. Employing large-scale density matrix renormalization group calculations, we obtain the phase diagram of a simple two-orbital model incorporating quantum geometric effect in a strong coupling regime. The phase diagram reveals a robust PDW phase with no coexisting competing orders across a broad range of doping concentration and tuning interaction parameter. The observed pairing field configuration aligns with the phenomenological understanding that quantum geometric effects promote PDW formation. Our study provides by far the strongest evidence for the quantum-geometry-facilitated intrinsic PDW order in strongly correlated systems, thereby opening an avenue for further exploration of PDWs.

Introduction.— Pair density waves (PDWs) are superconducting states exhibiting periodic modulation of the superconducting order parameter. A classic example of such a novel phase of matter is the Fulde-Ferrell-Larkin-Ovchinnikov state [1, 2], which may appear in BCS superconductors subject to external magnetic field. PDWs have also been reported in several strongly correlated systems, most notably the cuprate superconductors [3–8], although the exact mechanism for their formation is still debated [9, 10]. Meanwhile, PDW order in various microscopic models continues to be explored in great depth [11–37]. Recently, a possible new intrinsic route to PDW in absence of external field, utilizing the quantum geometric property of the paired electrons, was proposed for multiband superconductors [38, 39].

The quantum geometric effect can be understood in the following intuitive way. Specifically, the charge transport of electrons from different Bloch bands is quantum mechanically interconnected, rather than being solely determined by their respective group velocities. Formally, the current or velocity operator, when expressed in the band-basis representation, contains non-vanishing off-diagonal elements [40–42]:

$$V_{\mu\mathbf{k}}^{ij} = (\epsilon_{i\mathbf{k}} - \epsilon_{j\mathbf{k}}) \langle \partial_{k_\mu} \psi_{i\mathbf{k}} | \psi_{j\mathbf{k}} \rangle, \quad (\epsilon_{i\mathbf{k}} \neq \epsilon_{j\mathbf{k}}), \quad (1)$$

where i labels the band index, and $|\psi_{i\mathbf{k}}\rangle$ denotes the periodic part of the Bloch wavefunction of the i -th band, with its dispersion given by $\epsilon_{i\mathbf{k}}$. This interband velocity depicts a concerted motion of electrons from different bands. The term $i \langle \partial_{k_\mu} \psi_{i\mathbf{k}} | \psi_{j\mathbf{k}} \rangle$ defines a non-Abelian Berry connection between the two Bloch states. While the most classic examples of quantum geometric effects are found in the context of topological band theories [43–46], this effect, manifested through the interband velocity, is universally present in arguably any multiband system, regardless of the band topology.

The geometry also impacts the transport and electromagnetic responses of multiband superconductors [41, 42, 47–56]. For example, the superfluid weight, which measures the ability of Cooper pairs to maintain macroscopic phase coherence and hence to support supercurrent flow, receives a contribution closely related to the quantum geometry of the paired electrons [41, 47, 48, 57, 58]. This geometric superfluid weight has been invoked to explain the flatband superconductivity in several systems [47, 48, 57, 58], including in twisted bilayer graphene [59–63], where traditional theory would have otherwise concluded

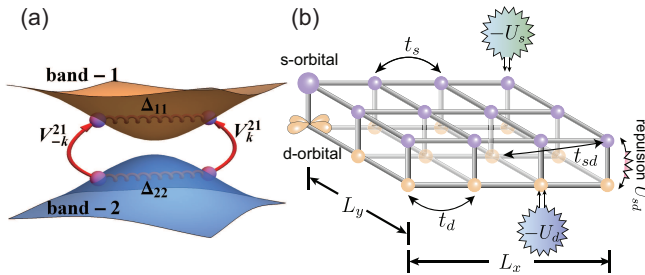


FIG. 1. (a) A representative manifestation of quantum geometric effects in multiband superconductors. Thanks to the interband velocity, Cooper pairs can tunnel between different Bloch bands, resulting in effective Josephson coupling between their order parameters. (b) Sketch of bilayer lattice model used in our DMRG simulation, with s and d_{xy} orbitals residing on separate layers. Details are provided in the text.

that superfluidity is unsustainable as the paired electrons in flatbands are immobile. Quantum geometry comes to the rescue, in the sense that interband velocity enables effective transport of Cooper pairs.

Quantum geometry also has the potential to facilitate the formation of unusual superconducting phases. One such example is the PDW order, as proposed by two independent recent studies within the framework of BCS mean-field theory [38, 39]. However, in the regime where PDW overtakes the uniform superconducting phase, the pairing gap typically reaches a magnitude comparable to or even larger than the Fermi energy and the bandwidth. This is a strong-coupling scenario, for which the applicability of the mean-field BCS formalism is in question. Hence, investigations using sophisticated many-body approaches are highly desired.

In this study, we perform large-scale density matrix renormalization group (DMRG) [64, 65] simulations of a simple non-topological interacting two-band model devised in Ref. 38 for the study of PDW facilitated by quantum geometry. Our numerical results reveal that PDW can indeed stabilize in the strong coupling limit. Our study therefore firmly establishes quantum geometry as an intrinsic mechanism to facilitate the formation of PDW phases.

Model and method.— The two-orbital model consists of an s - and a d_{xy} -orbital on a square lattice. The non-interacting part of the Hamiltonian is given by $H_0 = \sum_{\mathbf{k},\sigma} H_{0,\mathbf{k}}$ with,

$$H_{0,\mathbf{k}} = \xi_{s\mathbf{k}} c_{s\mathbf{k}}^\dagger c_{s\mathbf{k}} + \xi_{d\mathbf{k}} c_{d\mathbf{k}}^\dagger c_{d\mathbf{k}} + \lambda_{\mathbf{k}} (c_{s\mathbf{k}}^\dagger c_{d\mathbf{k}} + c_{d\mathbf{k}}^\dagger c_{s\mathbf{k}}). \quad (2)$$

Here, the dispersion relation $\xi_{\alpha\mathbf{k}} = -2t_\alpha (\cos k_x + \cos k_y)$ ($\alpha = s, d$ the orbital index) and $\lambda_{\mathbf{k}} = 4t_{sd} \sin k_x \sin k_y$, where $t_{s(d)}$ denotes the $s(d)$ -orbital nearest-neighbor intraorbital hopping and t_{sd} the next-neighbor interorbital mixing. For brevity, we omit the spin indices in Eq. (2), and henceforth refer to the d_{xy} -orbital as the d -orbital. Diagonalizing this Hamiltonian results in two bands, whose wavefunctions encode the geometric information crucial to the formation of PDW. Note that, this model is topologically trivial by nature, in the regard that the Berry curvature of the Bloch bands vanishes. In practice, we keep a balance between t_{sd} and $t_s - t_d$ to ensure a sizable quantum geometric effect. Without loss of generality, we set $t_s = -t_d = t_{sd} = 1$ throughout the study.

The interacting part of the Hamiltonian contains only onsite interactions. That is, $H_{\text{int}} = \sum_i H_{\text{int},i}$ where, on each site i ,

$$H_{\text{int},i} = -U_s c_{i,s\uparrow}^\dagger c_{i,s\downarrow}^\dagger c_{i,s\downarrow} c_{i,s\uparrow} - U_d c_{i,d\uparrow}^\dagger c_{i,d\downarrow}^\dagger c_{i,d\downarrow} c_{i,d\uparrow} + U_{sd} \left[c_{i,s\uparrow}^\dagger c_{i,s\downarrow}^\dagger c_{i,d\downarrow} c_{i,d\uparrow} + (s \leftrightarrow d) \right]. \quad (3)$$

Here, $-U_s, -U_d$ designate the attractive interactions that drive onsite intraorbital spin-singlet pairings Δ_s and Δ_d .

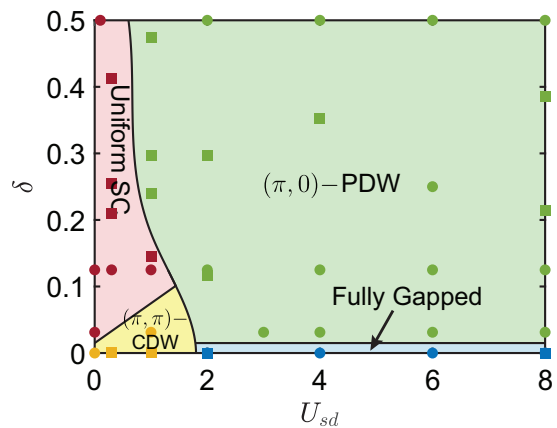


FIG. 2. The quantum phase diagram as a function of doping level δ and the inter-orbital repulsion U_{sd} is obtained from $L_y = 4$ DMRG calculations. The intra-orbital interaction strength is fixed at $U_s = U_d = 8$. Circles indicate calculations performed using canonical ensemble DMRG, while squares represent those gathered using grand canonical ensemble DMRG.

For strong interorbital pair hopping interaction U_{sd} , Δ_s and Δ_d tend to develop a phase difference of π , referred to as the $\hat{\Delta}_{+-}$ configuration. The alternative scenario with no phase difference is referred to as the $\hat{\Delta}_{++}$ configuration.

We employ a large-scale DMRG calculation to study the ground state properties of the above model. We map the Hamiltonian (2) and (3) into a bilayer square lattice model, with each layer representing one orbital degree of freedom [see Fig. 1 (b)]. The calculations are performed on a $L_x \times L_y$ system with open boundary conditions along the x -direction and periodic boundary conditions along the y -direction. The total number of sites is thus $N = 2 \times L_x \times L_y$. Data presented in the maintext are all $L_y = 4$, while we also perform some calculations with $L_y = 3$ to check consistency and present in Supplementary Material [66]. Simulating such a $L_y = 4$ ladder is computationally as demanding as simulating an 8-leg ladder of the single-orbital spinful model. Throughout the maintext, we focus on the strong coupling regime and set $U_s = U_d = 8$, which is computationally more accessible to us. We tune the value of U_{sd} and the doping level $\delta = 1 - \sum_{i,\alpha=s,d} n_{i,\alpha} / N > 0$ with $n_{i,\alpha}$ denoting the occupancy of the α -orbital on site i , to explore different phases of the model. Thanks to the particle-hole symmetry, we only need to study the hole-doped regime.

In this study, we utilize two types of DMRG techniques, each imposing distinct symmetry constraints: one preserving $U(1)_{\text{charge}} \otimes U(1)_{\text{spin}}$ symmetry and the other solely enforcing $U(1)_{\text{spin}}$ symmetry. The former, which can be referred to as the canonical ensemble, consistently prohibits a directly non-zero measurement of the superconductivity order parameter, namely, $\Delta \sim \langle c_{i,\sigma,\alpha}^\dagger c_{j,\sigma,\beta}^\dagger \rangle = 0$ at all times. In this case, the super-

conducting order can be only characterized by the correlation function. The latter, termed the grand canonical ensemble, naturally breaks particle number conservation at low entanglement condition and provides a non-zero estimate of the order parameter magnitude in the thermodynamic limit [25, 67–69]. These two methodologies serve as cross-checks for each other. In the canonical ensemble, we retain the bond dimension up to $D = 24000$, ensuring a truncation error $\varepsilon \sim 2 \times 10^{-6}$ for the PDW states. We also perform various simulations with different initial states to eliminate metastable states. All of the data from the canonical ensemble calculations presented below have been extrapolated to the $\varepsilon \rightarrow 0$ limit using quadratic fitting. Detailed numerical methods are provided in the Supplemental Materials [66].

Quantum-geometry-facilitated pair density wave order — Figure 2 presents a representative phase diagram as a function of doping concentration δ and pair hopping interaction U_{sd} for our model. The diagram reveals that the PDW phase dominates in a wide range of doping and pair hopping interactions, while a uniform superconducting phase develops at finite doping and small U_{sd} . At zero doping, a charge density wave (CDW) with momentum (π, π) initially stabilizes at low U_{sd} . As U_{sd} increases, this CDW phase transitions into a fully gapped phase that appears featureless.

We first concentrate on the PDW phase, which is the central result of this study. The robustness of superconductivity in our model is captured by the equal-time pair-pair correlation function defined as

$$\Phi_{\alpha\beta}(\mathbf{r} = \mathbf{r}_i - \mathbf{r}_j) = \langle \mathcal{O}_{\alpha,i}^\dagger \mathcal{O}_{\beta,j} \rangle, \quad (4)$$

where $\mathcal{O}_{\alpha,i}^\dagger = c_{\alpha,i,\uparrow}^\dagger c_{\alpha,i,\downarrow}^\dagger$ is the spin-singlet pair creation operator on site i with orbital index $\alpha = s, d$. To reduce boundary effects, the reference point \mathbf{r}_j is fixed at $\mathbf{r}_j = (x_j, y_j) = (L_x/4, 1)$ on the s -orbital. We first check

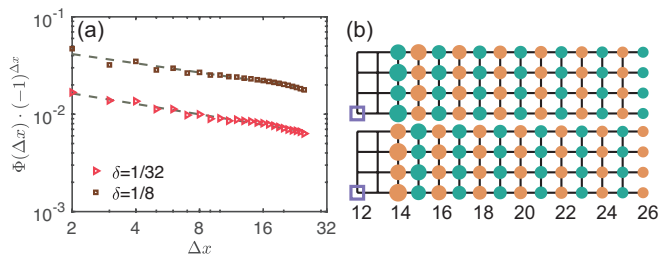


FIG. 3. SC Correlation functions in PDW phase. (a) SC correlations on s -orbital along the horizontal direction and their power-law fitting. (b) SC correlations on 4-leg ladder under doping level $\delta = 1/8$ plot in the quasi-2D lattices. The reference is set as the s -orbital intraorbital pairing on site $\mathbf{r}_0 = (12, 1)$. The upper panel is the correlation inner s -orbitals, the lower panel is the correlation between s - and d -orbitals. The area of the circle reflects the magnitude of SC correlations. The green circles indicate positive correlations, while the oranges ones indicate negative correlations.

for the presence of superconductivity. Figure 3(a) shows the pair-pair correlation function along the horizontal direction $\Phi(\Delta x) := \Phi_{ss}(\Delta x, \Delta y = 0)$ for two different points within the PDW phase, $U_{sd} = 8$ and $\delta = 1/8$ and $1/32$. The pair-pair correlation function exhibits characteristic power-law decay $\Phi(r) \propto r^{-K_{sc}}$ with Luttinger parameters $K_{sc} \simeq 0.36$ and 0.31 , respectively. The power-law decay with $K_{sc} < 2$ indicates a diverging superconducting susceptibility, establishing quasi-long-range superconducting order in our calculations. Moreover, as shown in the Supplementary Material [66], K_{sc} decreases as L_y increases from 3 to 4, suggesting stronger pairing as the ladder widens, thereby further consolidating the long-range PDW order in the two-dimensional limit. To our knowledge, the PDW order revealed here exhibits the strongest instability among all microscopic models confirmed by previous DMRG studies.

Figure 3(b) further illustrates the correlation $\Phi_{\alpha\beta}(\mathbf{r})$ across the lattice. The area and color of the filled circles encode the magnitude and sign of the correlation, respectively. The correlation function $\Phi_{\alpha\beta}(\mathbf{r})$ alternates in sign with a periodicity of two lattice sites along the x -direction and is translationally invariant along y . The PDW order, therefore, has a modulation wavevector $(\pi, 0)$. Notably, at each location \mathbf{r}_i , the signs of the intraorbital pairings on the two orbitals are opposite, corresponding to the $\hat{\Delta}_{+-}$ configuration. In all of our calculations, the PDW phase always appears in this configuration. This is consistent with the phenomenological analysis [38] that quantum geometric effects can facilitate the formation of the PDW phase.

The geometric effect is best illustrated in the band-basis description, which is obtained through a unitary transformation that diagonalizes the kinetic part of the Hamiltonian. In one exemplary manifestation of the geometric effect, Cooper pairs tunnel between the bands through the interband velocity, as exemplified in Fig. 1. Such tunnelings introduce effective Josephson couplings among the multiple pairing order parameters, which constitute a unique geometric superfluid weight. Importantly, the geometric contribution may acquire different signs [38, 39, 61, 70]. For example, changing the sign of the intraband order parameter on band-1 Δ_{11} in Fig. 1 changes the sign of the Josephson coupling between Δ_{11} and Δ_{22} and hence the sign of the corresponding portion of the geometric superfluid weight. If the total geometric contribution is negative, the energy cost associated with spatial superconducting phase modulations (*e.g.* PDW) can be significantly reduced.

Due to the strong orbital mixing t_{sd} in our model, the orbital-basis $\hat{\Delta}_{+-}$ pairing turns out to produce the right kind of band-basis order parameter configuration needed to generate negative geometric superfluid weight [38]. That is, had the $\hat{\Delta}_{+-}$ pairing develops into a uniform superconductivity in the sense that neither Δ_s nor Δ_d displays any spatial modulation, the system will receive

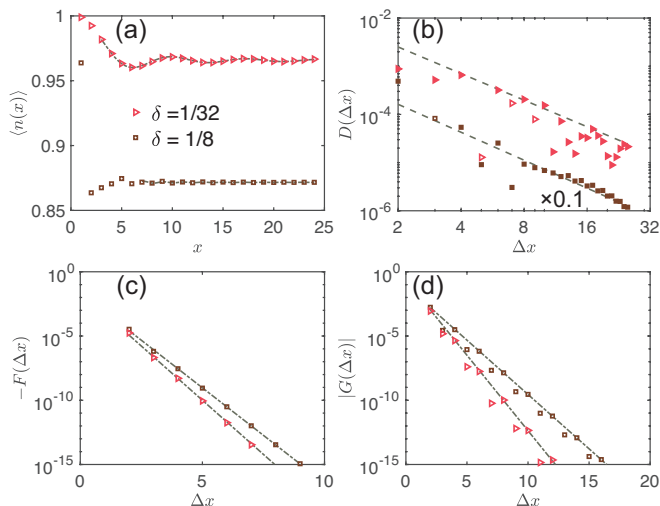


FIG. 4. Multiple correlation functions in the PDW phase. (a) Charge density profiles and Friedel oscillations. Only half of the systems are shown due to reflection symmetry. Charge density in s - and d -orbitals are degenerate due to the orbital exchange symmetry. (b) Charge density correlation functions inner s -orbitals and power law fitting. Data are scaled to separate different curves. Filled points indicate the negative values while empty points indicate positive values. (c) Spin correlation functions inner s -orbitals. (d) Single-particle correlation functions.

a negative geometry-related superfluid weight, thereby paving the way for PDW order to emerge. By contrast, as we will show later, when the repulsive pair hopping U_{sd} is weak, the system tends to condense into the $\hat{\Delta}_{++}$ configuration. The resultant state cannot produce negative geometric superfluid weight, and thus will not promote PDW order.

To check if there are other coexisting or competing instabilities, we also examine the possibility of charge and spin ordering. We first evaluate the charge density distribution $n_{\alpha}(x) = \frac{1}{L_y} \sum_y \langle \hat{n}_{\alpha}(x, y) \rangle$. It is checked that, similar to the PDW order, the charge density does not exhibit any modulation along the y direction. The density profile along x direction associated with the two calculations in Fig. 3 are shown in Fig. 4(a). Under the special parameters $t_s = -t_d$ and $U_s = U_d$, the density is exactly degenerate between two orbitals. With doping $\delta = 1/32$, on top of a large uniform component, one can see a clear oscillatory component whose amplitude rapidly decays going away from the open boundary. With doping $\delta = 0.125$, the oscillation is almost invisible in the bulk. The charge density modulations in $\delta = 1/32$ can be well described by the Friedel oscillations,

$$n^{\alpha}(x) = A \cos(Q \cdot r + \phi) x^{-K_c/2} + n_0 \quad (5)$$

where n_0 is the average density on the each orbital, Q is the charge modulation wavevector, A and ϕ are some non-universal constants, K_c is the Luttinger parameter.

By fitting the charge density profiles on $\delta = 1/32$, we obtain $Q \approx \frac{2\pi}{8}$ and Luttinger parameter $K_c \approx 2.94$. The values of Q indicates the scenario of $\frac{1}{L_y}$ -filled stripy charge density modulation.

These results provide preliminary indication of the absence of CDW instability in this part of the phase diagram. To substantiate this conclusion, we further measure the charge correlation function

$$D_{\alpha,\beta}(r) = \frac{1}{L_y} \sum_y \langle \hat{n}_{\alpha}(x_0, y) \hat{n}_{\beta}(x_0 + r, y) \rangle - \langle \hat{n}_{\alpha}(x_0, y) \rangle \langle \hat{n}_{\beta}(x_0 + r, y) \rangle. \quad (6)$$

The evaluated charge correlations for both orbitals (see Fig. 4(b) and Supplemental Materials [66]) show a power-law decay form $D_{\alpha\beta}(r) \sim r^{-K_c^{\alpha\beta}}$, with Luttinger parameter $K_c^{ss} \simeq 1.83, 1.95$ for the two calculations respective calculations. The power-law decay charge correlation, combined with the Friedel oscillations, offer strong evidence that the PDW phase is charge gapless and that CDW order, if any, must be significantly weaker than PDW.

The spin order can also be excluded in the PDW phase. This can be seen in the spin correlation function $F^{\alpha\beta}(r) = \frac{1}{L_y} \sum_{y=1}^{L_y} \langle \mathbf{S}_i^{\alpha} \cdot \mathbf{S}_j^{\beta} \rangle$. Figure 4 (c) presents exponentially decaying spin correlations, which are characterized by rather short spin correlation lengths of $\xi_s \approx 0.26, 0.29$ for the two calculations, suggesting large spin gap. We also calculate the single-particle correlation function $G(r) = \frac{1}{L_y} \sum_{y=1}^{L_y} \langle c^{\dagger}(x_0, y) c(x_0 + r, y) \rangle$, which also decay exponentially fast with correlation length $\xi_G \approx 0.37, 0.51$, indicating the presence of a single-particle gap in the PDW phase.

Considering the results from the above correlation functions, the PDW states qualitatively align with the scenario of Luther-Emery Liquids. Additionally, we present results of the PDW phase obtained for $L_y = 3$ and provide grand canonical ensemble calculations in the Supplementary Material [66]. A comprehensive analysis indicates that the PDW instability is the only one that is enhanced as the system width L_y increases.

Uniform SC, CDW and featureless phases — Having established and characterized the PDW phase, we now turn to the remaining phases in the phase diagram of Fig. 2. In Fig. 5 (a), we provide the charge density pattern for a representative set of parameters in the uniform superconducting phase, as well as the corresponding pairing potential $\langle c_{\alpha,i,\uparrow} c_{\alpha,i,\downarrow} \rangle$ obtained from a calculation with grand canonical ensemble. No CDW or pairing potential modulation is found in the bulk of the system. In the region that the repulsive pair hopping U_{sd} is small or absent, the order parameters Δ_s and Δ_d naturally condense into the $\hat{\Delta}_{++}$ configuration due to an effective Josephson coupling mediated by the orbital mixing t_{sd} . This configuration does not produce negative ge-

ometric superfluid weight [38], and thus cannot promote PDW order as we also confirmed in our calculations.

Figure 5 (c) shows the charge density pattern in the CDW phase at $U_{sd} = 0$ and at half-filling. The charge density modulates with wavevector (π, π) with uniform CDW amplitude in the bulk. And it exhibits an anti-phase correlation between two orbitals, *i.e.* the depletion and gain of the occupancy of the two orbitals alternates every other site, in concert with the CDW wavevector. We also checked that there is no coexisting SC or spin order in this phase. Finally, the fully-gapped phase at zero-doping is characterized by exact one electron per site and exponential decay in all channels of correlation functions [Fig. 5 (b)], which potentially holds a topological ordered phase. The exact nature of this intriguing phase requires further investigation, which is beyond the scope of the current study.

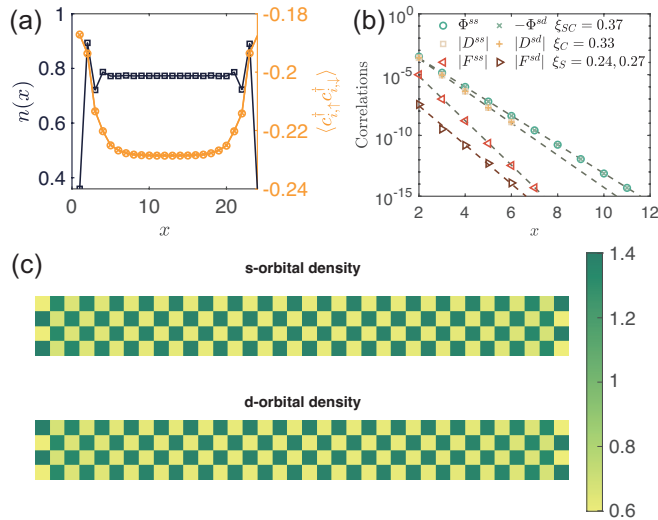


FIG. 5. (a) Charge density and SC pair-field in uniform SC phase. $U_{sd} = 0.3$. $\mu_s = \mu_d = -4.7$, equivalent to approximately doping level $\delta = 0.25$. The data are obtained from grand canonical ensemble DMRG with $D = 10000$ states. (b) Correlation functions at half filling and $U_{sd} = 8$. (c) Charge density pattern at half filling, $U_{sd} = 0$, showing a CDW with modulation wavevector (π, π) . Kept state $D = 20000$.

Concluding remarks.— With the use of large-scale DMRG calculations, we demonstrated a robust PDW order in the strong-coupling limit of a simple microscopic two-orbital model on a square lattice. This PDW forms only in the scenario where quantum geometric effects would induce a suppression in the superfluid weight of the uniform phase, which makes it easier for spatial superconducting modulation to take place. The model is topologically trivial, suggesting that band topology is not a prerequisite for this intrinsic geometric mechanism to operate. Intriguingly, the PDW wavevector obtained in our model is fixed at $(\pi, 0)$. Looking forward, it is worthwhile to explore the possibility of more general forms of

quantum-geometry-facilitated PDW order in other multi-orbital models with different lattice geometries and different schemes of interactions. Our study therefore opens an avenue for future explorations of PDW phases in strongly correlated multiband systems.

Acknowledgements We acknowledge helpful discussions with Shuai Chen, Zheng-Cheng Gu, Yi-Jian Hu, Wen Sun and Zheng Zhu. This work is supported by NSFC under grant No. 12374042 and No. 11904155, the Guangdong Science and Technology Department under Grant 2022A1515011948, and a Shenzhen Science and Technology Program (Grant No. KQTD20200820113010023). Computing resources are provided by the Center for Computational Science and Engineering at Southern University of Science and Technology. The DMRG code used to simulate the two-orbital model in this work is publicly available in Github [71].

* haoxinwang@cuhk.edu.hk

† huangw3@sustech.edu.cn

- [1] P. Fulde and R. A. Ferrell, Superconductivity in a strong spin-exchange field, Phys. Rev. **135**, A550 (1964).
- [2] A. I. Larkin and Y. N. Ovchinnikov, Nonuniform state of superconductors, Zh. Eksperim. i Teor. Fiz. **Vol: 47** (1964).
- [3] M. H. Hamidian, S. D. Edkins, S. H. Joo, A. Kostin, H. Eisaki, S. Uchida, M. J. Lawler, E.-A. Kim, A. P. Mackenzie, K. Fujita, J. Lee, and J. C. S. Davis, Detection of a Cooper-pair density wave in $\text{Bi}_2\text{Sr}_2\text{CaCu}_2\text{O}_{8+x}$, Nature **532**, 343 (2016).
- [4] W. Ruan, X. Li, C. Hu, Z. Hao, H. Li, P. Cai, X. Zhou, D.-H. Lee, and Y. Wang, Visualization of the periodic modulation of Cooper pairing in a cuprate superconductor, Nature Physics **14**, 1178 (2018).
- [5] S. D. Edkins, A. Kostin, K. Fujita, A. P. Mackenzie, H. Eisaki, S. Uchida, S. Sachdev, M. J. Lawler, E.-A. Kim, J. C. S. Davis, and M. H. Hamidian, Magnetic field-induced pair density wave state in the cuprate vortex halo, Science **364**, 976 (2019), <https://www.science.org/doi/pdf/10.1126/science.aat1773>.
- [6] Z. Du, H. Li, S. H. Joo, E. P. Donoway, J. Lee, J. C. S. Davis, G. Gu, P. D. Johnson, and K. Fujita, Imaging the energy gap modulations of the cuprate pair-density-wave state, Nature **580**, 65–70 (2020).
- [7] X. Li, C. Zou, Y. Ding, H. Yan, S. Ye, H. Li, Z. Hao, L. Zhao, X. Zhou, and Y. Wang, Evolution of charge and pair density modulations in overdoped $\text{Bi}_2\text{Sr}_2\text{CuO}_{6+\delta}$, Phys. Rev. X **11**, 011007 (2021).
- [8] J.-S. Lee, S. A. Kivelson, T. Wang, Y. Ikeda, T. Taniguchi, M. Fujita, and C.-C. Kao, Pair-density wave signature observed by x-ray scattering in La -based high- T_c cuprates (2023), arXiv:2310.19907 [cond-mat.supr-con].
- [9] E. Fradkin, S. A. Kivelson, and J. M. Tranquada, Colloquium: Theory of intertwined orders in high temperature superconductors, Rev. Mod. Phys. **87**, 457 (2015).
- [10] D. F. Agterberg, J. S. Davis, S. D. Edkins,

- E. Fradkin, D. J. Van Harlingen, S. A. Kivelson, P. A. Lee, L. Radzihovsky, J. M. Tranquada, and Y. Wang, The physics of pair-density waves: Cuprate superconductors and beyond, *Annual Review of Condensed Matter Physics* **11**, 231 (2020).
- [11] F. Liu and Z. Han, Pair density wave and $s \pm id$ superconductivity in a strongly coupled lightly doped kondo insulator, *Phys. Rev. B* **109**, L121101 (2024).
- [12] Z. Han, S. A. Kivelson, and H. Yao, Strong coupling limit of the holstein-hubbard model, *Phys. Rev. Lett.* **125**, 167001 (2020).
- [13] J. Wang, W. Sun, H.-X. Wang, Z. Han, S. A. Kivelson, and H. Yao, Pair density waves in the strong-coupling two-dimensional holstein-hubbard model: a variational monte carlo study (2024), arXiv:2404.11950 [cond-mat.str-el].
- [14] D. Shaffer and L. H. Santos, Triplet pair density wave superconductivity on the π -flux square lattice, *Phys. Rev. B* **108**, 035135 (2023).
- [15] D. Shaffer, F. J. Burnell, and R. M. Fernandes, Weak-coupling theory of pair density wave instabilities in transition metal dichalcogenides, *Phys. Rev. B* **107**, 224516 (2023).
- [16] Z. Wu, Y.-M. Wu, and F. Wu, Pair density wave and loop current promoted by van hove singularities in moiré systems, *Phys. Rev. B* **107**, 045122 (2023).
- [17] P. Castro, D. Shaffer, Y.-M. Wu, and L. H. Santos, Emergence of the chern supermetal and pair-density wave through higher-order van hove singularities in the haldane-hubbard model, *Phys. Rev. Lett.* **131**, 026601 (2023).
- [18] F. Liu, X.-X. Huang, E. W. Huang, B. Moritz, and T. P. Devereaux, Enhanced pair-density-wave vertices in a bilayer hubbard model at half-filling (2024), arXiv:2404.01389 [cond-mat.str-el].
- [19] N. S. Ticea, S. Raghu, and Y.-M. Wu, Pair density wave order in multiband systems (2024), arXiv:2403.00156 [cond-mat.supr-con].
- [20] F. Chen and D. N. Sheng, Singlet, triplet, and pair density wave superconductivity in the doped triangular-lattice moiré system, *Phys. Rev. B* **108**, L201110 (2023).
- [21] A. M. Tsvelik, Tractable model of a pair density wave, *Phys. Rev. B* **108**, 115129 (2023).
- [22] Y.-M. Wu, R. Thomale, and S. Raghu, Sublattice interference promotes pair density wave order in kagome metals, *Phys. Rev. B* **108**, L081117 (2023).
- [23] Z. Han and S. A. Kivelson, Pair density wave and reentrant superconducting tendencies originating from valley polarization, *Phys. Rev. B* **105**, L100509 (2022).
- [24] Z.-Y. Yue, Z.-T. Xu, S. Yang, and Z.-C. Gu, Pseudogap phase as fluctuating pair density wave (2024), arXiv:2404.16770 [cond-mat.str-el].
- [25] F. Chen, F. D. M. Haldane, and D. N. Sheng, D-wave and pair-density-wave superconductivity in the square-lattice t-j model (2023), arXiv:2311.15092 [cond-mat.supr-con].
- [26] P. A. Lee, Amperean pairing and the pseudogap phase of cuprate superconductors, *Phys. Rev. X* **4**, 031017 (2014).
- [27] Y.-M. Wu, P. A. Nosov, A. A. Patel, and S. Raghu, Pair density wave order from electron repulsion, *Phys. Rev. Lett.* **130**, 026001 (2023).
- [28] H.-K. Zhang, R.-Y. Sun, and Z.-Y. Weng, Pair density wave characterized by a hidden string order parameter, *Phys. Rev. B* **108**, 115136 (2023).
- [29] C. Setty, J. Zhao, L. Fanfarillo, E. W. Huang, P. J. Hirschfeld, P. W. Phillips, and K. Yang, Exact solution for finite center-of-mass momentum cooper pairing, *Phys. Rev. B* **108**, 174506 (2023).
- [30] H.-C. Jiang, Pair density wave in the doped three-band hubbard model on two-leg square cylinders, *Phys. Rev. B* **107**, 214504 (2023).
- [31] H.-C. Jiang and T. P. Devereaux, Pair density wave and superconductivity in a kinetically frustrated doped emery model on a square lattice, *Frontiers in Electronic Materials* **3**, 10.3389/femat.2023.1323404 (2023).
- [32] J.-T. Jin, K. Jiang, H. Yao, and Y. Zhou, Interplay between pair density wave and a nested fermi surface, *Phys. Rev. Lett.* **129**, 167001 (2022).
- [33] A. Banerjee, C. Pépin, and A. Ghosal, Charge, bond, and pair density wave orders in a strongly correlated system, *Phys. Rev. B* **105**, 134505 (2022).
- [34] X.-Y. Song, Y.-H. Zhang, and A. Vishwanath, Doping a moiré mott insulator: A $t-j$ model study of twisted cuprates, *Phys. Rev. B* **105**, L201102 (2022).
- [35] Y.-F. Jiang and H. Yao, Pair density wave superconductivity: a microscopic model in two dimensions (2023), arXiv:2308.08609.
- [36] X. Zhu, J. Sun, S.-S. Gong, W. Huang, S. Feng, R. T. Scalettar, and H. Guo, Exact demonstration of pair-density-wave superconductivity in the σ_z -hubbard model (2024), arXiv:2404.11043.
- [37] K. S. Huang, Z. Han, S. A. Kivelson, and H. Yao, Pair-density-wave in the strong coupling limit of the holstein-hubbard model, *npj Quantum Materials* **7** (2020).
- [38] W. Chen and W. Huang, Pair density wave facilitated by Bloch quantum geometry in nearly flat band multiorbital superconductors, *Science China Physics, Mechanics & Astronomy* **66**, 287212 (2023).
- [39] G. Jiang and Y. Barlas, Pair density waves from local band geometry, *Phys. Rev. Lett.* **131**, 016002 (2023).
- [40] E. I. Blount, Formalisms of band theory, in *Solid State Physics*, Vol. 13, edited by D. T. Frederick Seitz (Elsevier, 1962) pp. 305–373.
- [41] L. Liang, T. I. Vanhala, S. Peotta, T. Siro, A. Harju, and P. Törmä, Band geometry, berry curvature, and superfluid weight, *Phys. Rev. B* **95**, 024515 (2017).
- [42] W. Chen and W. Huang, Quantum-geometry-induced intrinsic optical anomaly in multiorbital superconductors, *Phys. Rev. Res.* **3**, L042018 (2021).
- [43] D. J. Thouless, M. Kohmoto, M. P. Nightingale, and M. den Nijs, Quantized hall conductance in a two-dimensional periodic potential, *Phys. Rev. Lett.* **49**, 405 (1982).
- [44] X.-L. Qi and S.-C. Zhang, Topological insulators and superconductors, *Rev. Mod. Phys.* **83**, 1057 (2011).
- [45] D. Xiao, M.-C. Chang, and Q. Niu, Berry phase effects on electronic properties, *Rev. Mod. Phys.* **82**, 1959 (2010).
- [46] M. Z. Hasan and C. L. Kane, Colloquium: Topological insulators, *Rev. Mod. Phys.* **82**, 3045 (2010).
- [47] S. Peotta and P. Törmä, Superfluidity in topologically nontrivial flat bands, *Nature Communications* **6**, 8944 (2015).
- [48] A. Julku, S. Peotta, T. I. Vanhala, D.-H. Kim, and P. Törmä, Geometric origin of superfluidity in the lieb-lattice flat band, *Phys. Rev. Lett.* **117**, 045303 (2016).
- [49] M. Iskin, Exposing the quantum geometry of spin-orbit-coupled fermi superfluids, *Phys. Rev. A* **97**, 063625 (2018).

- [50] M. Iskin, Geometric mass acquisition via a quantum metric: An effective-band-mass theorem for the helicity bands, *Phys. Rev. A* **99**, 053603 (2019).
- [51] Z. Wang, G. Chaudhary, Q. Chen, and K. Levin, Quantum geometric contributions to the bkt transition: Beyond mean field theory, *Phys. Rev. B* **102**, 184504 (2020).
- [52] J. Ahn and N. Nagaosa, Superconductivity-induced spectral weight transfer due to quantum geometry, *Phys. Rev. B* **104**, L100501 (2021).
- [53] T. Kitamura, S. Kanasugi, M. Chazono, and Y. Yanase, Quantum geometry induced anapole superconductivity, *Phys. Rev. B* **107**, 214513 (2023).
- [54] M. Chazono, S. Kanasugi, T. Kitamura, and Y. Yanase, Piezoelectric effect and diode effect in anapole and monopole superconductors, *Phys. Rev. B* **107**, 214512 (2023).
- [55] S. A. Chen and K. T. Law, Ginzburg-landau theory of flat-band superconductors with quantum metric, *Phys. Rev. Lett.* **132**, 026002 (2024).
- [56] J.-L. Zhang, W. Chen, H.-T. Liu, Y. Li, Z. Wang, and W. Huang, Quantum-geometry-induced anomalous hall effect in nonunitary superconductors and application to Sr_2RuO_4 , *Phys. Rev. Lett.* **132**, 136001 (2024).
- [57] P. Törmä, S. Peotta, and B. A. Bernevig, Superconductivity, superfluidity and quantum geometry in twisted multilayer systems, *Nature Reviews Physics* **4**, 528 (2022).
- [58] P. Törmä, Essay: Where can quantum geometry lead us?, *Phys. Rev. Lett.* **131**, 240001 (2023).
- [59] X. Hu, T. Hyart, D. I. Pikulin, and E. Rossi, Geometric and conventional contribution to the superfluid weight in twisted bilayer graphene, *Phys. Rev. Lett.* **123**, 237002 (2019).
- [60] A. Julku, T. J. Peltonen, L. Liang, T. T. Heikkilä, and P. Törmä, Superfluid weight and berezinskii-kosterlitz-thouless transition temperature of twisted bilayer graphene, *Phys. Rev. B* **101**, 060505 (2020).
- [61] F. Xie, Z. Song, B. Lian, and B. A. Bernevig, Topology-bounded superfluid weight in twisted bilayer graphene, *Phys. Rev. Lett.* **124**, 167002 (2020).
- [62] H. Tian, X. Gao, Y. Zhang, S. Che, T. Xu, P. Cheung, K. Watanabe, T. Taniguchi, M. Randeria, F. Zhang, C. N. Lau, and M. W. Bockrath, Evidence for dirac flat band superconductivity enabled by quantum geometry, *Nature* **614**, 440–444 (2023).
- [63] J.-X. Hu, S. A. Chen, and K. T. Law, Anomalous coherence length in superconductors with quantum metric (2023), arXiv:2308.05686.
- [64] S. R. White, Density matrix formulation for quantum renormalization groups, *Phys. Rev. Lett.* **69**, 2863 (1992).
- [65] S. R. White, Density-matrix algorithms for quantum renormalization groups, *Phys. Rev. B* **48**, 10345 (1993).
- [66] See Supplemental Material for additional data in pair-density wave phase (Sec. I), support data for the uniform superconductivity states (Sec. II), as well as some DMRG technical details (Sec. III).
- [67] S. Jiang, D. J. Scalapino, and S. R. White, Ground-state phase diagram of the t - J model, *Proceedings of the National Academy of Sciences* **118**, e2109978118. <https://www.pnas.org/doi/pdf/10.1073/pnas.2109978118>.
- [68] S. Jiang, D. J. Scalapino, and S. R. White, Pairing properties of the t - t' - t'' - j model, *Phys. Rev. B* **106**, 174507 (2022).
- [69] S. Jiang, D. J. Scalapino, and S. R. White, Density matrix renormalization group based downfolding of the three-band hubbard model: Importance of density-assisted hopping, *Phys. Rev. B* **108**, L161111 (2023).
- [70] T. Kitamura, A. Daido, and Y. Yanase, Quantum geometric effect on fulde-ferrell-larkin-ovchinnikov superconductivity, *Phys. Rev. B* **106**, 184507 (2022).
- [71] <https://github.com/QuantumLiquids/UltraDMRG>; <https://github.com/QuantumLiquids/Quantum-geometry-facilitated-PDW-DMRG>.

SUPPLEMENTAL MATERIALS

I. SUPPLEMENTARY DATA FOR PAIR-DENSITY WAVE STATES

We present extra DMRG calculation results in this section to support the robustness of the pair density wave (PDW) states.

A. 3-leg ladders

The computational capacity limits our system size to $L_y \leq 4$. To carefully extrapolate the model behavior in the two-dimensional (2D) limit, we compare the numerical results from $L_y = 3$ and $L_y = 4$. Thus, in this file, we present some results for $L_y = 3$ under different doping levels δ and different interaction strength. Throughout this file, we set $t_s = -t_d = t_{sd} = 1$ as in the main text.

We first present the results for a 3-leg ladder with $U_s = U_d = U_{sd} = 8$ at doping level $\delta = 1/8$, directly comparing these results with those for a 4-leg ladder with the same parameters as discussed in the main text. Figure S1 (a) shows the charge density distribution calculated using several increasingly larger sets of DMRG kept states. We note three observations from the density distributions: (i) The distributions do not converge around the boundary region with respect to the kept states but are consistent in the bulk. (ii) The average charge density in the bulk is approximately

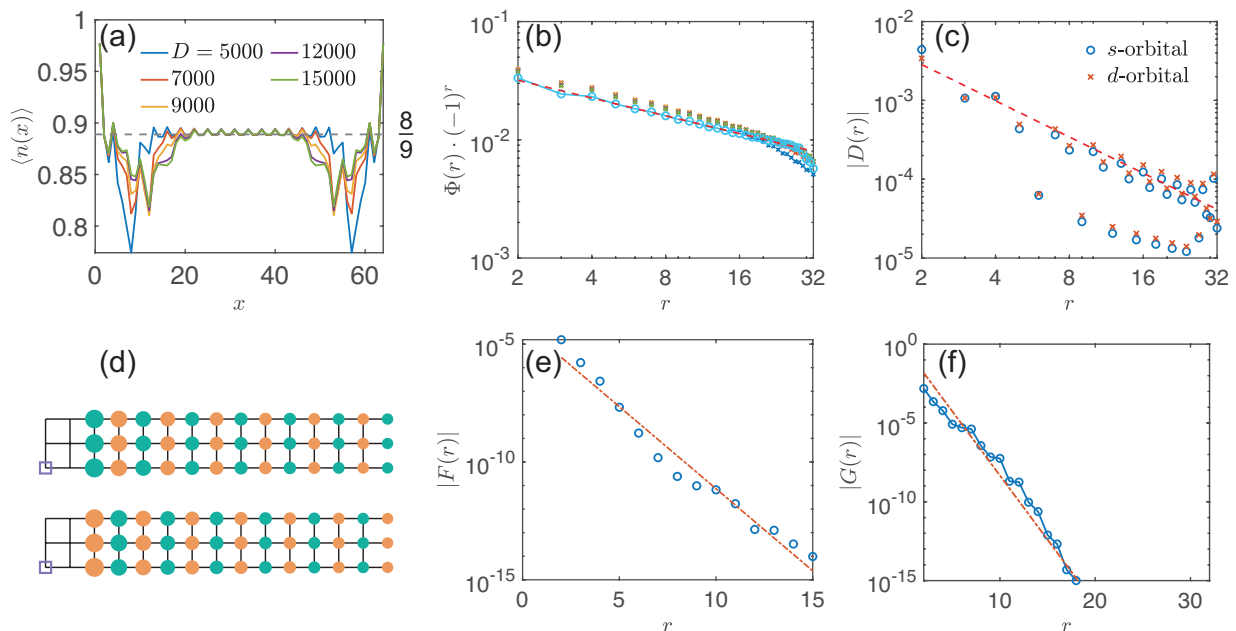


FIG. S1. Numerical results of a 3×64 lattice with model parameters: $U_s = U_d = U_{sd} = 8$, and doping level $\delta = 1/8$. (a) Charge density pattern at various finite bond dimensions D . (b) SC correlations at finite bond dimension and extrapolation. (c) Charge density correlations. (d) Real-space SC correlations with the reference set as the s -orbital intraorbital pairing on site $\mathbf{r}_0 = (16, 1)$. The area of the circle reflects the magnitude of SC correlations. The green circles indicate positive correlations, while the orange ones indicate negative correlations. (e) and (f) show the spin and single-particle correlations.

$8/9$, corresponding to a doping level of $\delta = 1/9$. (iii) There is a small charge density wave (CDW) modulation with a period of $\lambda_{\text{CDW}} = 3$. The doping level $\delta = 1/9$ in the bulk can also be confirmed by the prior belief that the stripe filling is $1/L_y$ in the PDW phase, which has been observed in other cases. These three observations suggest that under this set of parameters, the model on a 3-leg ladder ($L_y = 3$) tends to form phase separation. We also obtain that the following correlations measured in the bulk of the system reflect the behavior at a doping level $\delta = 1/9$.

We measured the SC, charge, spin, and single-particle correlations, as shown in Fig. S1(b-f). The behavior of the correlation functions is consistent with that in $L_y = 4$ systems. We again observe a $(\pi, 0)$ -PDW with a power-law decay in the SC correlation. The charge mode is gapless, characterized by a power-law decay in the charge correlation. The spin and single-particle degrees of freedom are all gapped and characterized by exponential decay correlations. The SC and density correlations give Luttinger parameters $K_{sc} = 0.50$ and $K_c = 1.52$, respectively. Here, the tails of the SC and density correlations slightly deviate from the dashed guideline due to the phase separation.

From the above calculations, we conclude that a strong PDW phase appears in the $L_y = 3$ system under these parameters. The Luttinger parameter K_{sc} is larger than that in the $L_y = 4$ system discussed in the main text with doping levels $\delta = 1/8$ and $1/32$, suggesting that the SC becomes stronger as L_y increases, thus further indicating the presence of long-range SC order in the 2D limit.

To further explore regions with relatively weaker interactions, we examine the calculation results for $t_s = -t_d = t_{sd} = 1$ and $U_s = 3.8$, $U_d = 3.7$, $U_{sd} = 4.0$, as shown in Figure S2. The mean-field solution for these parameters has been considered in Ref. [37] and indicates a $(\pi, 0)$ -PDW order in the ground state. The results here are qualitatively similar to the PDW state investigated in the strong interaction regime.

The charge density wave (CDW) shows clear Friedel oscillations and decaying CDW amplitudes as one moves into the bulk of the system, with a modulation periodicity $\lambda_{\text{CDW}} = \frac{16}{3}$, giving a stripe filling of $\frac{1}{L_y}$. The quasi-long-range $(\pi, 0)$ -PDW and density correlations provide Luttinger parameters $K_{sc} = 0.53$ and $K_c = 1.94$, respectively. The K_c fitted from the density correlation is consistent with that fitted from the Friedel oscillation up to two decimal places. Given the fact that both spin and single-particle modes are gapped, the product $K_{sc}K_c \approx 1$ strongly indicates a Luther-Emery liquid state in this regime.

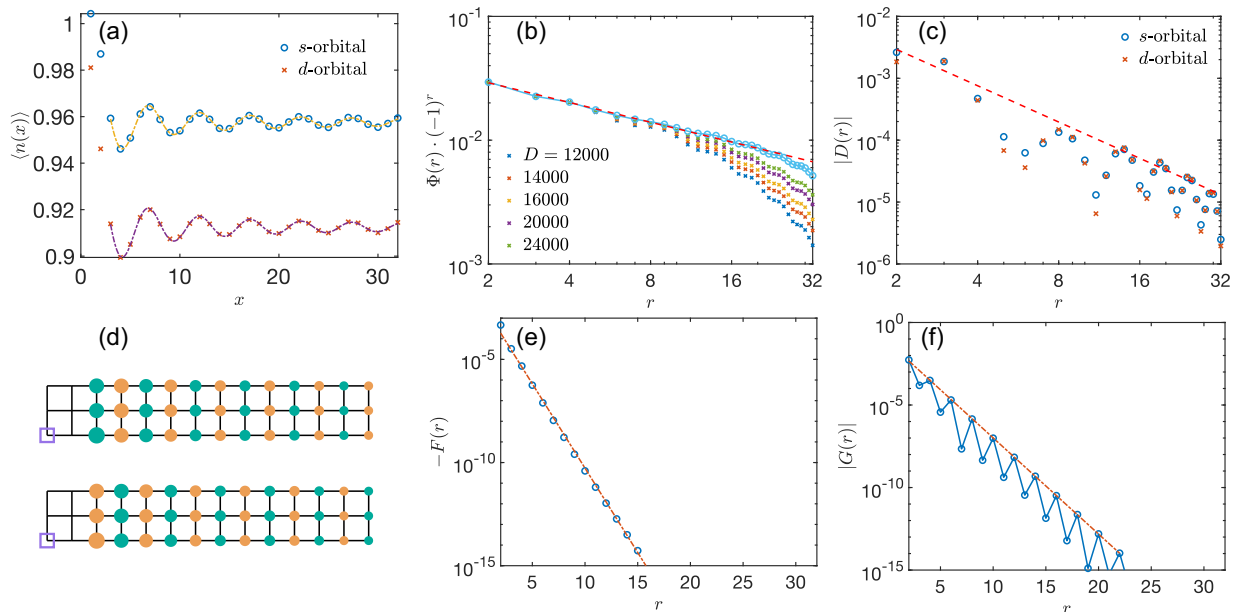


FIG. S2. Correlations on a 3×64 lattice. Model parameters: $U_s = 3.8$, $U_d = 3.7$, $U_{sd} = 4.0$, and doping level $\delta = 1/16$. (a) Charge density profile and Friedel oscillation. (b) SC correlations. (c) Charge density correlations. (d) SC correlations a 2D top-view representation. (e) Spin correlation. (f) Single-particle correlation.

B. Grand canonical ensemble DMRG simulation

The existence of the PDW phase is further confirmed by the grand canonical ensemble DMRG simulation. To adjust the doping level, we add a chemical potential term $-\mu_s \hat{N}_s - \mu_d \hat{N}_d$ to the Hamiltonian, where \hat{N}_s and \hat{N}_d represent the total particle numbers in the s - and d -orbitals, respectively. We demonstrate a representative point in the phase diagram with model parameters $U_s = U_d = 8$, $U_{sd} = 4$, and $\mu_s = \mu_d = -6$, as shown in Figure S3. The doping level for this set of parameters is approximately 0.35.

The charge density distribution reveals no CDW in the ground state [Figure S3 (a)]. The on-site pairing field $\langle c_{i,\uparrow,\alpha}^\dagger c_{i,\downarrow,\alpha}^\dagger \rangle$, shown in Figure S3 (b), exhibits a $(\pi, 0)$ -PDW modulation, consistent with the PDW correlation measured in the canonical ensemble. The pairing fields between different layers exhibit a phase difference, forming the $\hat{\Delta}_{+-}$ configuration, which facilitates the formation of the PDW. Additionally, we plot the dependence of the on-site pairing field strength on the bond dimension D in Figure S3 (c). The "shoulder" strongly indicates the leading instability of the SC order [25, 65].

II. ESTABLISHMENT OF UNIFORM SUPERCONDUCTIVITY IN THE SMALL- U_{sd} REGION

Due to space limitations, we previously did not provide sufficient data to support the existence of uniform superconductivity in the small U_{sd} region. In this section, we present representative results illustrating the uniform superconducting (SC) states in the phase diagram. All data presented here are gathered from $L_y = 4$ systems.

Before presenting the results, we discuss a technical detail. As the system transitions from the PDW phase to the uniform phase by decreasing U_{sd} , the truncation error in DMRG calculations abruptly increases from the order of 10^{-6} to 10^{-4} , indicating a phase transition nearby. However, this increase in truncation error also makes the calculations more difficult to converge. With truncation errors of this magnitude, the extrapolation of the correlation function may not be reliable. Therefore, we need to carefully analyze the raw data of the correlations.

We show the charge and SC properties of the uniform SC states in Fig. S4. We choose model parameters $\delta = 1/8$ and $U_{sd} = 0$ or 0.3 from the phase diagram in Figure 2. The charge density exhibits no apparent modulation for both parameters, indicating the absence of CDW order. While the SC correlations decay exponentially under finite bond dimensions, they visibly enhance with increasing bond dimension. We fit the SC correlation lengths and plot their dependence on the bond dimensions in Fig. S4(e). The dependence of the correlation length on the bond dimensions can be well fitted by $\xi \propto D^\alpha$, with $\alpha = 0.39$ and 0.36 for the respective cases. This suggests that the SC correlation

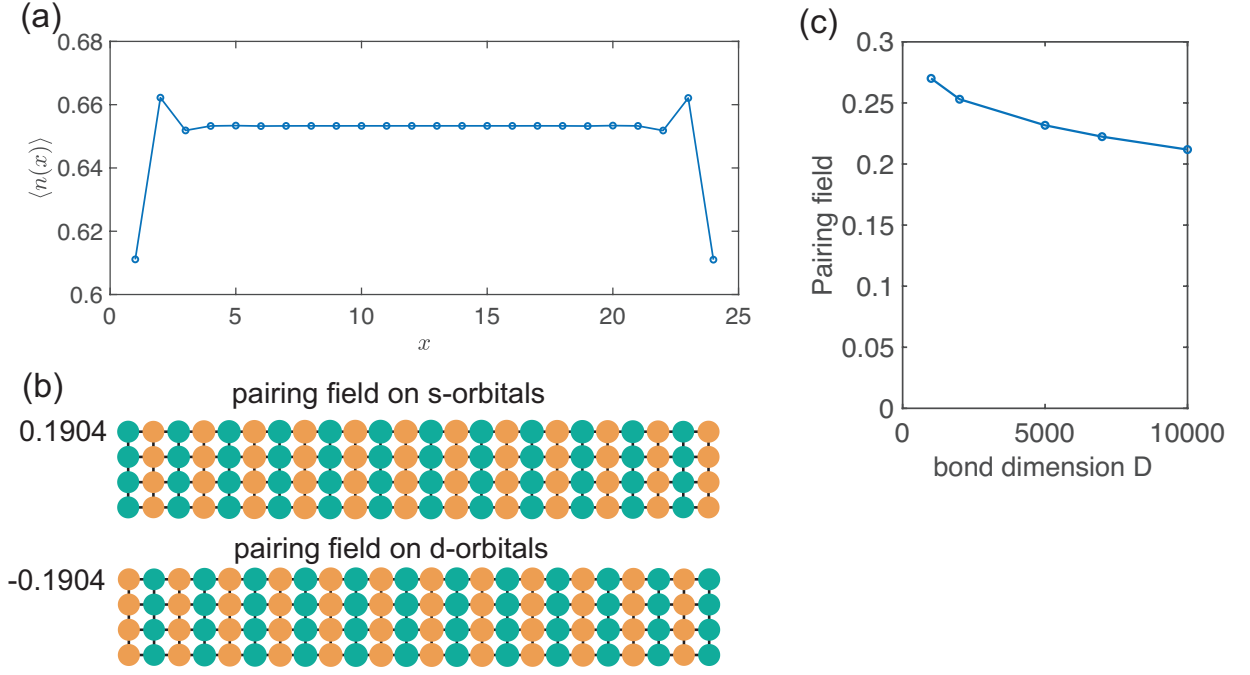


FIG. S3. Charge density and SC pairing field calculated in the grand canonical ensemble. Model parameters: $U_s = U_d = 8$, $U_{sd} = 4$, $\mu_s = \mu_d = -6$, corresponding to a doping level $\delta \approx 0.35$. (a) Charge density pattern for kept state $D = 10000$. (b) SC pairing field. (c) The magnitude of SC pairing field vs. DMRG kept state D .

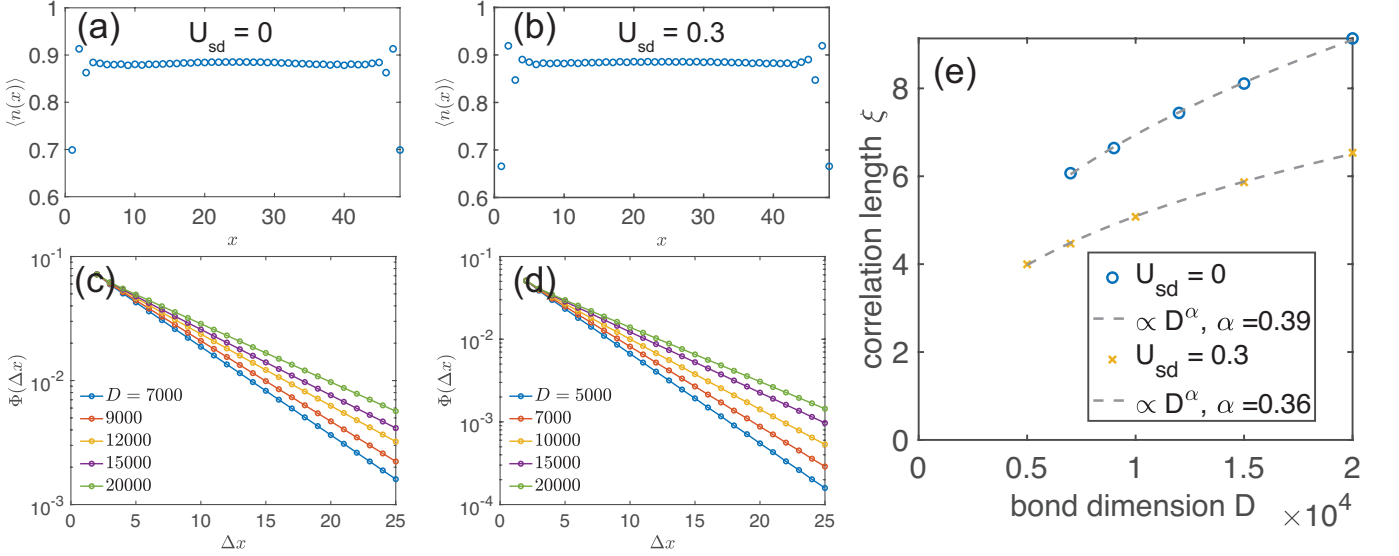


FIG. S4. Charge density pattern and SC correlation calculated in the uniform SC phase. The model parameters are chosen from the phase diagram in Figure 2 in the main text, with doping level $\delta = 1/8$ and $U_{sd} = 0$ or 0.3. (a,b) show the charge density pattern. (c,d) show the SC correlation in the s -orbital obtained by a series of gradually increasing DMRG bond dimensions. (e) shows the bond dimension dependence of the SC correlation length ξ .

may diverge at the infinite bond dimension. Assuming that the SC correlations decay in a power-law manner at infinite bond dimension, a brute-force power-law fitting of the correlations at $D = 20000$ yields an upper bound estimation for the Luttinger parameter $K_{sc} \leq 0.74$ and $K_{sc} \leq 1.21$.

The existence of uniform superconductivity (SC) has also been confirmed by grand canonical ensemble calculations, as shown in Fig. 5(a) in the main text. Here, we present the corresponding bond dimension dependence of the pairing field strength in Fig. S5. In the figure, we include two additional sets of calculations under different chemical

potentials. For the cases with $\mu_s = \mu_d = -4.6$ or -4.7 , the pairing field strength exhibits a "shoulder" behavior [25, 65]. For the case with $\mu_s = \mu_d = -5$, the pairing field strength increases as the bond dimension D increases. All these cases indicate the leading instability toward uniform SC order.

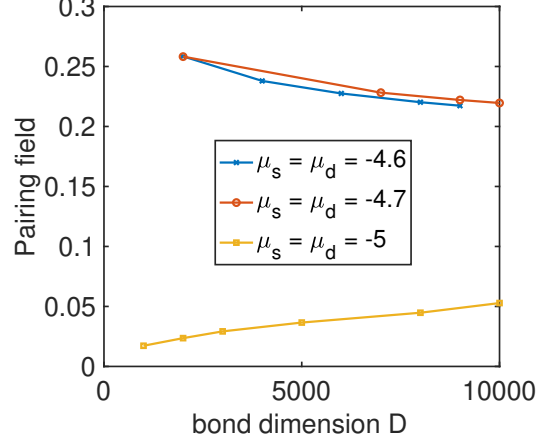


FIG. S5. The magnitude of uniform SC pairing field *v.s.* DMRG bond dimension D . $U_s = U_d = 8$, and $U_{sd} = 0.3$.

III. DATA EXTRAPOLATIONS IN DMRG

We use a quadratic function to extrapolate the expectation values in DMRG calculations. We denote $A(\epsilon)$ as the truncation error dependence of the measurement results for the observable \hat{A} with successively changing bond dimension D . The extrapolated measurement $A(0)$, corresponding to the infinite bond dimension, is obtained by quadratic fitting as follows:

$$A(\epsilon) = A(0) + b\epsilon + c\epsilon^2. \quad (\text{S1})$$